An automatic classification technique for attenuation correction in positron emission tomography

V. Bettinardi[1], E. Pagani[1], M.C. Gilardi[1], C. Landoni[1], C. Riddell[1], G. Rizzo[1], I. Castiglioni[1], D. Belluzzo[1], G. Lucignani[1], S. Schubert[2], F.Fazio[1]

[1] INB-CNR, Scientific Institute H San Raffaele, University of Milan, Italy
[2] GE Medical System, Milwaukee,Wisconson, USA

Received 8 August and in revised form 29 December 1998

Abstract. In this paper a clustering technique is proposed for attenuation correction (AC) in positron emission tomography (PET). The method is unsupervised and adaptive with respect to counting statistics in the transmission (TR) images. The technique allows the classification of pre- or post-injection TR images into main tissue components in terms of attenuation coefficients. The classified TR images are then forward projected to generate new TR sinograms to be used for AC in the reconstruction of the corresponding emission (EM) data. The technique has been tested on phantoms and clinical data of brain, heart and whole-body PET studies. The method allows: (a) reduction of noise propagation from TR into EM images, (b) reduction of TR scanning to a few minutes (3 min) with maintenance of the quantitative accuracy (within 6%) of longer acquisition scans (15–20 min), (c) reduction of the radiation dose to the patient, (d) performance of quantitative whole-body studies.

Key words: Attenuation correction – Clustering technique – Position emission tomography

Eur J Nucl Med (1999) 26:447–458

Introduction

Attenuation of annihilation photons in the patient's body is commonly compensated in positron emission tomography (PET) by transmission (TR) measurements of attenuation correction (AC) factors, using an external radioactive source. AC factors are calculated as the pixel by pixel ratio of a blank scan, acquired before positioning the patient in the scanner field of view, and a TR scan performed with the patient in position. AC is obtained by multiplying the emission (EM) sinogram of the radioactivity distribution and the resulting sinogram of AC factors. A drawback recognised in the measured AC technique is the propagation of the statistical noise, present in the TR data, into the EM images, reducing PET quantitative accuracy [1–3]. For this reason, TR scans have to be acquired for a length of time sufficient to enable the collection of enough counts to limit the statistical noise in the TR data. Depending on the radioactivity present in the external source and on the dimension and composition of the body under investigation, TR scans usually last for 15–30 min. On the other hand, an acquisition time as short as possible would be desirable, given that TR and EM scans have to be perfectly aligned to allow accurate AC and the patient has to be motionless during the whole PET study. In particular, a short TR acquisition time is mandatory when repeated PET scans at multiple bed positions are acquired to cover an extended part of the body as in whole-body studies, which are currently performed without AC.

Several methods have been proposed with the aim of improving measured AC, reducing the time for the acquisition of TR scans and of the PET study [4–22]. While measured AC based on post-injection TR acquisitions, performed either simultaneously [4–7] or immediately after [8–14] the EM scan, is effective in avoiding or reducing the problem of TR/EM misalignment, it does not bring about an improvement in terms of the statistical noise in TR images. A promising approach consists in performing TR measurements by a single-photon instead of the coincidence acquisition technique, allowing high statistics TR data to be collected within a short acquisition time (a few minutes) [15]. Unfortunately, as the use of single-photon sources causes high dead-time problems and requires specially designed hardware, this technique cannot be straightforwardly implemented on every PET scanner. A different approach is to apply off-line image processing methods to short TR scans, in order to reduce statistical noise. Various techniques have been proposed. In particular, Xu et al. [17] suggest the use of an automatic thresholding method for the segmen-

Correspondence to: F. Fazio, Department of Nuclear Medicine, Scientific Institute H San Raffaele, Via Olgettina 60, I-20132 Milan, Italy

tation of short TR images into two classes: soft tissue (including bones) and lungs (including patient couch). Within the two thresholded regions the average value of the attenuation coefficient is calculated and then assigned to each segmented region. Meikle et al. [20] have proposed a modification of the aforementioned method: three components (air, lung and soft tissue) are identified in the TR data by fitting the histogram of the attenuation values with gaussian functions and assigning each pixel to a specific component by a maximum likelihood rule. In the technique suggested by Tai et al. [21], the contours of the lungs and of the external body are identified on TR and EM images respectively. Two classes are recognised accordingly (lungs and soft tissue) and the average attenuation coefficient is assigned to each segmented region. A two step procedure has been proposed by Xu et al. [22]: (a) an optimal thresholding technique is applied for an initial classification of the TR images into two classes, to which a fixed attenuation coefficient is assigned (0.095 cm^{-1} for the soft tissue and 0.035 cm^{-1} for the lungs); (b) intermediate values of the attenuation coefficients are then assigned by re-inserting the original values with different weights for the two segmented classes.

In this work, we propose a clustering method for the classification of TR images into the main tissue components with the aim of reducing noise in very short TR scans. The main characteristics of this technique with respect to the previous image processing methods are:

1. It is unsupervised with respect to the number of clusters and their centroid values (no a priori assumption is made).
2. It is adaptive with respect to the statistical noise in the TR images.
3. It is adaptive with respect to the body regions under evaluation (head, body).

Clustering technique

Technique and its implementation

The clustering technique considered in this work has been proposed for general image processing applications by G. Beni and X. Liu as a new least biased fuzzy clustering method [23].

The basic and only assumption of the method is that "the centroids have no bias towards any of the data points". This assumption can be mathematically described as:

$$\sum_{i=1}^{N}(x_i - c)\,p_i(x_i,c) = 0, \tag{1}$$

where: i = index for the data point, N = number of data points in the image, x_i = data point and $p_i(x_i, c)$ = clustering membership. Probability for the centroid c to cluster the data point x_i.

The clustering membership $p_i(x_i, c)$ is normalised to 1 over all the data points in the image. $p_i(x_i, c)$ can be expressed as:

$$p_i(x_i,c) = \frac{\exp\left[-\beta D(x_i,c)\right]}{\sum_{j=1}^{N}\exp\left[-\beta D(x_j,c)\right]}, \tag{2}$$

where: $D(x_i, c)$ = distance function between x_i and c, β = scale parameter and j = index for the data point.

Considering Eqs. 1 and 2, one can obtain:

$$c = \sum_{i=1}^{N} x_i p_i(x_i,c) = \frac{\sum_{i=1}^{N} x_i \exp\left[-\beta D(x_i,c)\right]}{\sum_{j=1}^{N}\exp\left[-\beta D(x_j,c)\right]}. \tag{3}$$

Equation 3 can be iteratively solved as:

$$c^{(n+1)} = \sum_{i=1}^{N} x_i p_i(x_i, c^{(n)}), \tag{4}$$

where: n = iteration number.

The method is unsupervised, making no assumption with regard to the number of clusters or their centroid values. The technique uses an iterative procedure and produces different classification results by using different values for the scale parameter β. As stated by Beni and Liu, "convergence to a same fixed point it is not guaranteed by starting from an arbitrary location. However, by choosing the initial location to coincide with a data point, the convergence is unambiguous for a given resolution parameter β used".

In this work the technique was implemented and adapted for use in for the classification of PET TR data in a clinical environment. Characteristics of this implementation with respect to the original one are as follows:

– the scale parameter β is calculated using an empirical formulation which relates the parameter β to the count statistics in the TR data for each image section (see section "Adaptive behaviour of the clustering technique")

– all calculations are performed on a histogram base and not on a cluster (pixel) base. Using the histogram approach, Eq. 1 and Eq. 3 can be rewritten as:

$$\sum_{k=0}^{H} h(k)(k-c)\,p(k,c) = \sum_{k=0}^{H} h(k)(k-c)\frac{\exp\left[-\beta|k-c|\right]}{\sum_{l=0}^{H} h(l)\exp\left[-\beta|l-c|\right]}, \tag{5}$$

and

$$c = \sum_{k=0}^{H} h(k)k\,p(k,c) = \sum_{k=0}^{H} h(k)k\frac{\exp\left[-\beta|k-c|\right]}{\sum_{l=0}^{H} h(l)\exp\left[-\beta|l-c|\right]}, \tag{6}$$

where: k = index for the grey level, l = index for the grey level, H = number of grey levels, $h(k)$ = number of data points with the grey level k, c = cluster centre and $p(k,c)$ = probability for the centroid c to cluster the data point with grey level k.

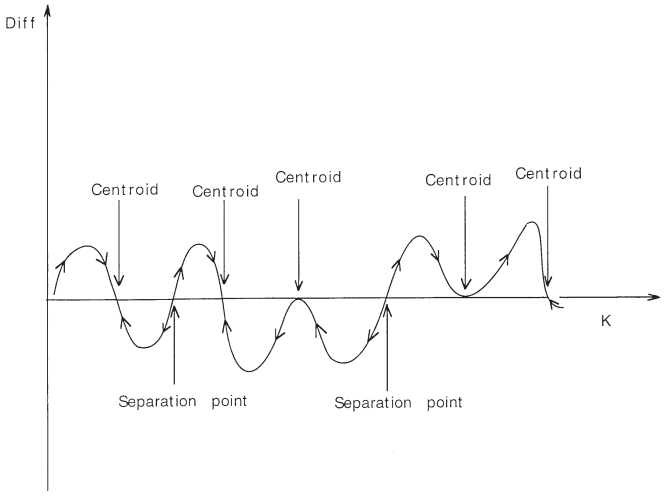

Fig. 1. Classification technique: graphical representation of the cluster identification

– search for the cluster centres is performed by solving Eq. 6 using a graphical method associated with the iterative approach.

Using the graphical method the solutions of Eq. 6 are found searching for symmetries in the grey level histogram of the TR image with respect to each bin of the histogram itself. Data partitioning is then obtained by relating each cluster to a centroid, described as an actractor point for that cluster. Graphically the solutions of Eq. 6 can be represented by the points at the intersection between the straight line represented by $y = c$ and the curve described by the function at the right side of Eq. 6. The actractor centroids are located in transitions from negative to positive (moving from left to right) of the difference between the straight line and the function, while transitions from positive to negative represent repulsive or separation points between classes (Fig. 1). For all the transitions which include an actractor, in order to define the centroid position, the iterative procedure is started from the one of the two points closer to the transition. Convergence is accepted when the distance between the centroid position at two consecutive iterations is less than 10^{-4}. Critical points where the solution is not clearly represented by the intersection between the straight line and the function (e.g. tangent) are solved using a "distance approach": if the distance between the line and the function is less than 10^{-4}, then the point is accepted as solution for Eq. 6.

Figure 1 graphically shows how each data point is assigned to a specific centroid (see arrows).

Data processing – from raw to classified TR sinograms

Classification of PET TR images and generation of classified TR sinograms is performed according to the following procedure:

1. Normalisation of blank and TR sinograms to account for non-uniformity in detector response.
2. Filtering of blank and TR sinograms (row by row) using a monodimensional gaussian function (full-width at half maximum, FWHM =8 mm).
3. Calculation of the natural log of the pixel by pixel ratio between blank and TR sinograms.
4. Reconstruction of TR images on 128×128 image matrices using a filtered back-projection algorithm with Hanning filter (cut-off: 0.5 cycles/pixel). The reconstructed TR images represent in each pixel the linear attenuation coefficient (μ) expressed in cm^{-1}.
5. Removal of the head holder or bed in the reconstructed TR images by reading (in the file header) the absolute spatial position where the acquisition was performed and then using a predefined mask region to set to zero all the pixels within the mask.
6. Removal of the background noise, typical of filtered back-projection reconstruction algorithms, using a "cleaning" algorithm, which scans each TR image row by row and column by column along the x and y directions from both sides from outside towards the centre of the matrix. When the intensity of a pixel is lower than a predefined threshold value ($\mu = 0.035\ cm^{-1}$), it is set to zero. When a pixel with intensity equal to or higher than the threshold is found, the edge of the object is recognised and scanning for that row or column is stopped. The choice of the threshold value was based on the analysis of the background level in very short TR scans (maximum background value increases from $\approx 0.005\ cm^{-1}$ to $\approx 0.030\ cm^{-1}$ for TR scanning times from 5 to 1 min respectively).
7. Generation of the histogram of "grey levels". The attenuation coefficient represented in each pixel of the reconstructed TR image is multiplied by 10^3 and then ordered in a histogram with a bin step of 1.
8. Classification of the TR images using the clustering algorithm with a selected β value.
9. Filtering of the classified TR images by convolution with a gaussian function (FWHM = 4 mm). Filtering was applied to remove sharp transitions between different regions possibly occurring in the classified images and to degrade classified TR images to the effective system spatial resolution.
10. Re-insertion of the head holder (or bed) in the processed TR images in the proper position. A high count statistics TR image of the head holder (or bed), acquired once, is used instead of the original as noise-free reference data.
11. Forward projection and pixel by pixel exponentiation of the resulting matrix. The resulting sinogram is a classified TR sinogram of AC factors to be used for AC of the corresponding EM data.

PET scanner

The PET tomograph used in this study was the GE-Advance scanner (General Electric Medical System, Milwaukee, Wis.). The system consists in 12096 bismuth germanate (BGO) crystals organised in 18 rings. The

crystals have dimensions of 4.0 mm transaxially, 8.1 mm axially and 30 mm radially. A detection unit (block) consists of 6×6 crystals, coupled to two double photomultipliers. The 18 crystal rings allows 35 two-dimensional (2D) images to be obtained, spaced by 4.25 mm, covering an axial field of view of 15.2 cm. The system has tungsten septa 1 mm thick and 12 cm long. The septa, which define the image planes in 2D scanning mode, can be automatically retracted to allow radiation detection in three-dimensional (3D) scanning mode. TR data can be recorded using a pair of germanium-68 pin sources, which can be automatically positioned in the scanner field of view and rotated around the longitudinal axis of the scanner. At the time of this work the activity in the two pin TR sources was ~6.8 mCi (251.6 MBq)/pin. For each PET study a blank scan of 45 min was acquired.

Phantom studies: set up of the classification technique

Data acquisition

The anthropomorphic phantom Rando Anderson [24] was used to evaluate the classification technique. TR scans of 60, 30, 15, 5 and 3 min were acquired for the chest and the head regions respectively.

Data analysis

TR data were processed and reconstructed according to the clustering procedure described above, in the section "Data processing – from raw to classified TR sinograms". As in this case the analysis is performed only on TR images, steps 10 and 11 were not applied. β values of 3.0, 2.5, 2.0, 1.5, 1.0, 0.8, 0.6 and 0.4 were used for the classification of TR images.

Classified TR images and high statistics 60-min unclassified TR images (assumed as reference) were analysed as follows: Irregular regions of interest (ROIs) were drawn in the main anatomical regions of both chest (soft tissue and lungs) and head (brain tissue and skull) TR studies. Mean values of attenuation coefficients μ and standard deviations (SD), representative of the image noise, were calculated for each set of ROIs (soft tissue, lungs, bone etc.).

Results

Two representative slices of the Rando phantom (at the level of the chest and the abdomen) for the original and the classified TR studies (using different β values) are shown in Fig. 2. It can be observed that the use of "high" β values (e.g. >1.0) results in classified images very similar to the original ones; in particular for $\beta = 2$ the images are almost identical. This correspond to generate a relatively high number of classes, meaning, in the spatial domain, that "small" details and transitions between regions with different μ can be preserved in the processed TR images, although without complete removal of the original noise. "Low" β values (e.g. <1.0) are more effective in removing noise, but with loss of "small" details in the classified images (in particular near the interfaces between liver and lungs) and generation of sharp transitions between regions with different μ, corresponding to a few well-defined main classes. Figure 3 shows, as an example, the different behaviour of the algorithm in terms of number of classes found during the classification of a TR image using a "high" (1.5) and a "low" (0.8) β value.

This qualitative visual assessment of the performance of the clustering procedure is confirmed by the ROI analysis. Mean μ values and SD calculated in the main anatomical regions are reported in Tables 1 and 2 for the chest and brain regions respectively. As a result of the algorithm behaviour, mean μ values and SD for $\beta = 2$ also can be considered as representative for the original TR images. In the chest region, differences within 2%, in terms of mean μ value, were obtained in soft tissue over all the classification configurations considered with respect to the 60-min unprocessed TR images (reference data). A maximum error of 4% was found in the lung tissue for short acquisition scans (<5 min) and for a low β value (0.4). In the head region, while the algorithm performs well in the soft tissue, a problem is recognised in its capability to differentiate the skull from the brain tissue. Errors of up to 8.6% ($\beta = 0.4$) were found in this case.

Adaptive behaviour of the clustering technique

The results described in the preceding section suggested that the clustering technique should be modified in order to:

– Improve the classification technique to make it adaptive with respect to the body region (two-step procedure for the head)

– Improve the classification technique to make it adaptive with respect to count statistics in TR data.

Steps 1–7 and 9–11 of the procedure described in the section "Data processing – from raw to classified TR sinograms" in section 2.2 were unchanged, while step 8 was modified and split into two steps (8a and 8b), as described below:

Step 8a. Before the application of the classification technique the maximum linear dimension (MLD) of the object (in the *x* direction) is calculated in each TR image. The MLD is used to differentiate the head from other body regions.

– Head region: identification and classification.

The first head section is recognised where the MLD is greater than 1 pixel and less than 60 pixels (pixel size = 4.3 mm). Subsequent sections which verify the

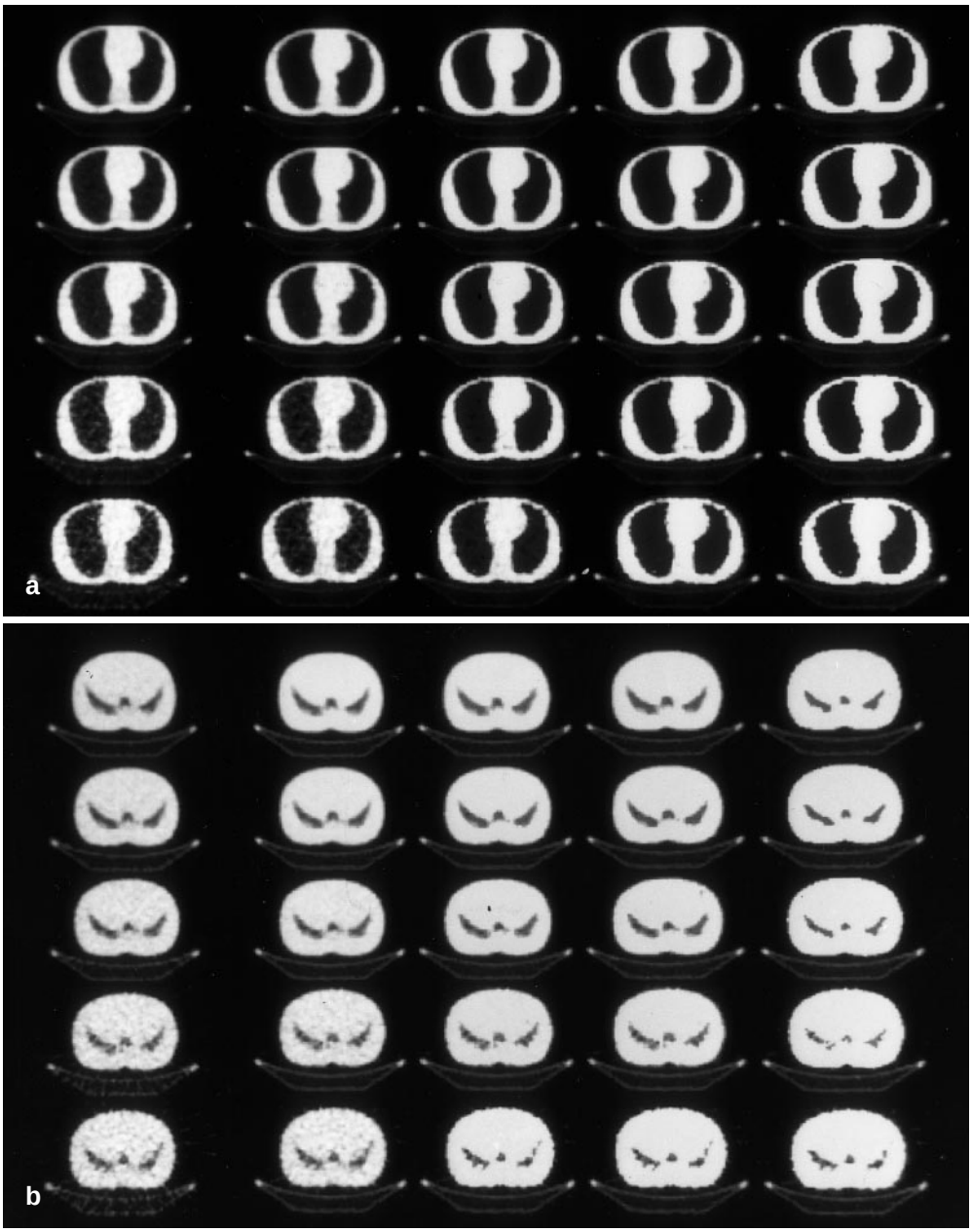

Fig. 2. a Rando phantom (chest region). Unprocessed (first column) and classified TR images as a function of the acquisition time (60, 30, 15, 5, 3 min – *from top to bottom*) and β values used for the classification (β = 2.0, 1.0, 0.8, 0.4 from the second column, *left to right*). **b** Rando phantom (abdomen region). Unprocessed (first column) and classified TR images as a function of the acquisition time (60, 30, 15, 5, 3 min – *from top to bottom*) and β values used for the classification (β = 2.0, 1.0, 0.8, 0.4 from the second column, *left to right*)

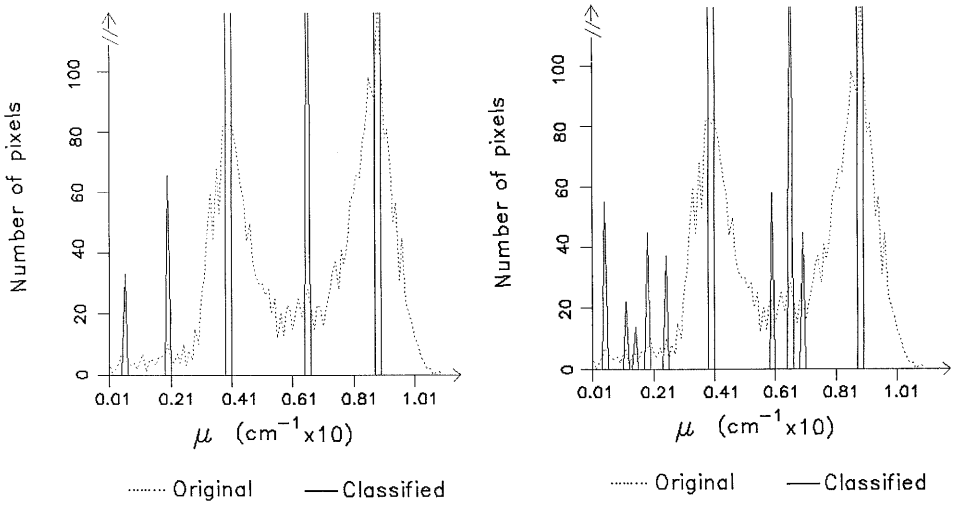

Fig. 3. Rando phantom (chest region). Original (*broken line*) and classified (*solid line*) histograms obtained using β = 0.8 (*left*), β = 1.5 (*right*)

Table 1. Rando phantom (chest region): Mean values and (SD) of the attenuation coefficients ($cm^{-1}\times1000$) as calculated for ROIs drawn in the soft tissue and lung as a function of the acquisition time (Acq-T, min) and the β values used in the classification of the TR images. Reference values were calculated from the unprocessed high statistics (60-min) TR images

Acq-T (min)	β=3	β=2.5	β=2.0	β=1.5	β=1.0	β=0.8	β=0.6	β=0.4
Soft tissue								
60	90.4 (2.3)	90.3 (1.9)	90.4 (1.0)	90.5 (0.4)	90.6 (0.1)	90.5 (0.1)	90.3 (0.0)	89.9 (0.0)
30	90.5 (2.9)	90.2 (2.5)	90.1 (1.7)	90.2 (0.5)	90.2 (0.2)	90.2 (0.1)	90.1 (0.0)	89.9 (0.0)
15	90.6 (3.9)	90.6 (3.7)	90.1 (2.7)	90.2 (1.2)	90.1 (0.2)	90.2 (0.1)	90.0 (0.0)	89.8 (0.0)
5	91.2 (6.5)	91.2 (6.4)	90.6 (6.0)	90.5 (5.2)	89.9 (1.2)	89.6 (0.5)	89.5 (0.2)	89.3 (0.1)
3	91.6 (8.6)	91.5 (8.5)	91.3 (8.3)	90.7 (7.0)	89.8 (2.6)	89.5 (1.3)	89.0 (0.7)	88.9 (0.6)
Lung								
60	29.3 (2.3)	29.4 (2.0)	29.5 (1.4)	29.4 (0.5)	29.4 (0.1)	29.5 (0.0)	29.6 (0.0)	29.8 (0.0)
30	29.2 (3.0)	29.4 (2.7)	29.7 (1.9)	29.5 (1.2)	29.2 (0.2)	29.3 (0.0)	29.8 (0.0)	29.8 (0.0)
15	29.4 (3.8)	29.5 (3.6)	29.9 (2.9)	30.2 (1.2)	30.1 (0.3)	30.1 (0.0)	30.1 (0.0)	30.2 (0.0)
5	29.7 (6.2)	29.7 (6.0)	29.8 (5.9)	30.2 (4.8)	30.4 (2.2)	30.5 (0.9)	30.6 (0.3)	30.6 (0.0)
3	29.6 (7.9)	29.6 (7.6)	29.7 (7.5)	29.7 (7.1)	29.8 (4.8)	30.3 (3.2)	30.3 (2.0)	29.8 (0.0)

Reference value for soft tissue: 90.6 (2.6)
Reference value for lung: 29.4 (2.7)

Table 2. Rando phantom (head region): Mean values and (SD) of the attenuation coefficients ($cm^{-1}\times1000$) as calculated for ROIs drawn in the skull and soft tissue as a function of the acquisition time (Acq-T, min) and the β values used in the classification of the TR images. Reference values were calculated from the unprocessed high statistics (60-min) TR images

Acq-T (min)	β=3	β=2.5	β=2.0	β=1.5	β=1.0	β=0.8	β=0.6	β=0.4
Skull								
60	100.7 (4.2)	100.3 (4.0)	99.0 (3.9)	94.6 (1.8)	93.3 (0.3)	92.8 (0.2)	92.7 (0.0)	92.7 (0.0)
30	100.8 (4.5)	100.6 (4.5)	99.2 (4.1)	93.5 (1.4)	93.0 (0.3)	92.9 (0.2)	92.7 (0.1)	92.7 (0.0)
15	100.8 (5.5)	100.6 (5.4)	99.8 (5.0)	96.1 (2.8)	93.3 (0.3)	93.2 (0.2)	93.3 (0.1)	93.3 (0.0)
5	100.9 (6.2)	100.8 (6.1)	100.3 (5.8)	98.2 (3.7)	94.0 (1.2)	94.0 (0.3)	94.0 (0.0)	93.8 (0.0)
3	101.5 (7.9)	101.5 (7.9)	101.2 (7.6)	99.7 (6.4)	96.3 (1.6)	95.4 (0.5)	95.3 (0.2)	94.8 (0.0)
Soft tissue								
60	91.6 (1.7)	91.7 (1.3)	91.8 (0.5)	91.9 (0.1)	92.0 (0.0)	92.1 (0.0)	92.2 (0.0)	92.2 (0.0)
30	91.6 (2.6)	91.8 (2.0)	92.2 (0.9)	92.2 (0.2)	92.3 (0.0)	92.4 (0.0)	92.4 (0.0)	92.3 (0.0)
15	91.7 (4.6)	91.8 (4.3)	92.2 (3.3)	92.2 (1.8)	92.5 (0.0)	92.7 (0.0)	92.7 (0.0)	92.8 (0.0)
5	92.0 (6.2)	91.7 (1.3)	92.3 (5.4)	92.7 (3.3)	93.0 (0.9)	92.9 (0.4)	92.9 (0.2)	93.0 (0.0)
3	92.8 (8.2)	92.8 (8.1)	92.8 (7.7)	92.9 (6.4)	93.9 (2.6)	94.1 (0.6)	94.5 (0.0)	94.2 (0.0)

Reference value for skull: 101.5 (4.4)
Reference value for soft tissue: 91.4 (2.2)

same condition are included in the head region. No more than 35 consecutive slices are accepted as the head region. Once the head region has been defined, a first raw classification is performed using a β value of 0.4.

As a second step, the edge of the head and the sharp μ transitions (e.g. the nose cavity) are recognised using a window mask (7×7 pixels). Every time not all the pixels in the window have the same μ, the μ value of the corresponding central pixel in the unprocessed data is stored in a new image. At the end, two subimages of the head are generated (Fig. 4). A second classification is performed on these two subimages using an optimised β value as described in the next step (8b). The two classified subimages are then merged to yield a single final classified image.

– Other body regions: identification and classification. All the slices where the MLD is greater than 60 pixels. As for the head, a first raw classification is performed using a low β value of 0.4. A second classification is then performed using an optimised β value as described in the next step (8b).

Step 8b: β selection. An empirical formulation was implemented to allow an adaptive behaviour of the algorithm with respect to the count statistics in the TR data. Following the first classification, all the pixels that have

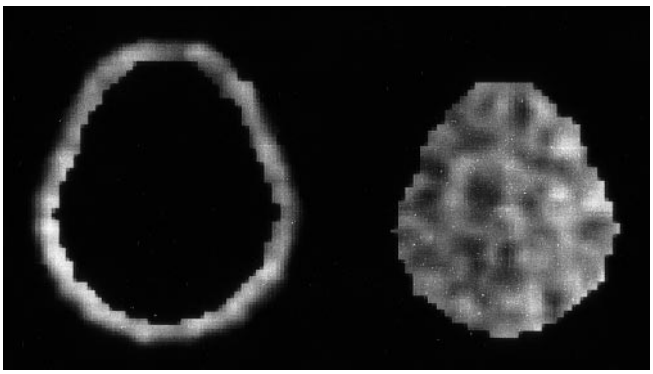

Fig. 4. Rando phantom (head region). Two unprocessed subimages (skull and soft tissue) as resulting from the two-step procedure used for the classification of the head

been classified as soft tissue are sampled from the original data (before classification) and the resulting histogram is fitted with a gaussian function. The SD of this gaussian function is used to estimate the β value to be used in the classification.

Considering Eq. 5, the term which mainly controls the degree to which the choice of a centre *c* is affected by the surrounding points is $(k–c)\ \exp(–\beta|k–c|)$, which can be seen as a function $f(i) = i\ \exp(–\beta|i|)$.

The function $f(i)$, which is odd, acts on the histogram as a window which selects the histogram range beyond which the contribution to the sum is practically negligible. Based on this, β is imposed so that $f(i)$ goes to zero after 2SD:

$$2SD\exp(-\beta|2SD|)=\varepsilon, \quad (7)$$

with $\varepsilon=10^{-6}$.

Table 4. Rando phantom: mean β values calculated as a function of the noise (SD) in the 35 TR images

Acquisition time (min)	β chest region	β head region
60	2.2	2.5
30	1.8	2.0
15	1.4	1.3
5	0.8	1.1
3	0.7	0.9

In this way, the parameter β can be related to the SD of the noise as follows:

$$\beta = -\ln\left(\frac{\varepsilon}{2SD}\right)\frac{1}{2SD}. \quad (8)$$

Results using the adaptive procedure

Table 3 summarises the results (in terms of μ values and SD) obtained using the two-step procedure for the head region of the Rando phantom. A representative image (original and classified) of the Rando phantom (head) obtained using the two-step procedure is shown in Fig. 5. The two-step procedure allows a more accurate classification to be obtained, in particular for the skull, where the maximum error is reduced to 5.2%.

The β values calculated for the Rando phantom data using the adaptive procedure are reported in Table 4. It can be observed that adaptive β values decrease accounting for count statistics in TR data. Using these β values, as can be extrapolated from Table 1 for chest and Table 3 for brain, classification errors are within maximum

Table 3. Rando phantom (head region): Mean values and (SD) of the attenuation coefficients ($cm^{-1}\times1000$) as calculated, using the two-step procedure, for ROIs drawn in the skull and soft tissue as a function of the acquisition time (Acq-T, min), and the β values used in the classification of the TR images using teh two-step procedure. Reference values were calculated from the unprocessed high statistics (60-min) TR images

Acq-T (min)	β=3	β=2.5	β=2.0	β=1.5	β=1.0	β=0.8	β=0.6	β=0.4
Skull								
60	100.7 (4.2)	100.3 (3.9)	99.9 (3.5)	99.5 (2.9)	99.2 (2.0)	98.7 (1.3)	98.1 (1.0)	98.1 (1.0)
30	100.8 (4.5)	100.6 (4.3)	100.1 (4.1)	99.2 (3.6)	98.6 (2.5)	98.3 (2.1)	98.2 (1.8)	97.9 (1.5)
15	100.7 (5.5	100.7 (5.5)	100.5 (5.2)	99.6 (4.3)	97.9 (2.4)	98.1 (1.9)	97.9 (1.4)	97.6 (1.1)
5	100.9 (6.3)	100.3 (3.9)	100.7 (6.0)	99.7 (5.1)	98.3 (2.9)	97.9 (2.3)	97.8 (1.6)	97.6 (1.3)
3	101.5 (7.9)	101.5 (7.9)	101.4 (7.7)	100.8 (7.1)	98.6 (5.1)	96.8 (3.3)	96.6 (2.4)	96.5 (1.4)
Soft tissue								
60	91.6 (1.7)	91.7 (1.3)	91.8 (0.5)	91.9 (0.1)	92.0 (0.0)	92.1 (0.0)	92.2 (0.0)	92.2 (0.0)
30	91.6 (2.6)	91.8 (2.0)	92.2 (0.9)	92.2 (0.2)	92.3 (0.0)	92.4 (0.0)	92.4 (0.0)	92.3 (0.0)
15	100.7 (5.5)	100.7 (5.5)	100.5 (5.2)	99.6 (4.3)	97.9 (2.4)	98.1 (1.9)	97.9 (1.4)	97.6 (1.1)
15	91.7 (4.6)	91.8 (4.3)	92.2 (3.3)	92.2 (1.8)	92.5 (0.0)	92.7 (0.0)	92.7 (0.0)	92.8 (0.0)
5	92.0 (6.2)	91.7 (1.3)	92.3 (5.4)	92.7 (3.3)	93.0 (0.9)	92.9 (0.4)	92.9 (0.2)	93.0 (0.0)
3	92.8 (8.2)	92.8 (8.1)	92.8 (7.7)	92.9 (6.4)	93.9 (2.6)	94.1 (0.6)	94.5 (0.0)	94.2 (0.0)

Reference value for skull: 101.5 (4.4)
Reference value for soft tissue: 91.4 (2.2)

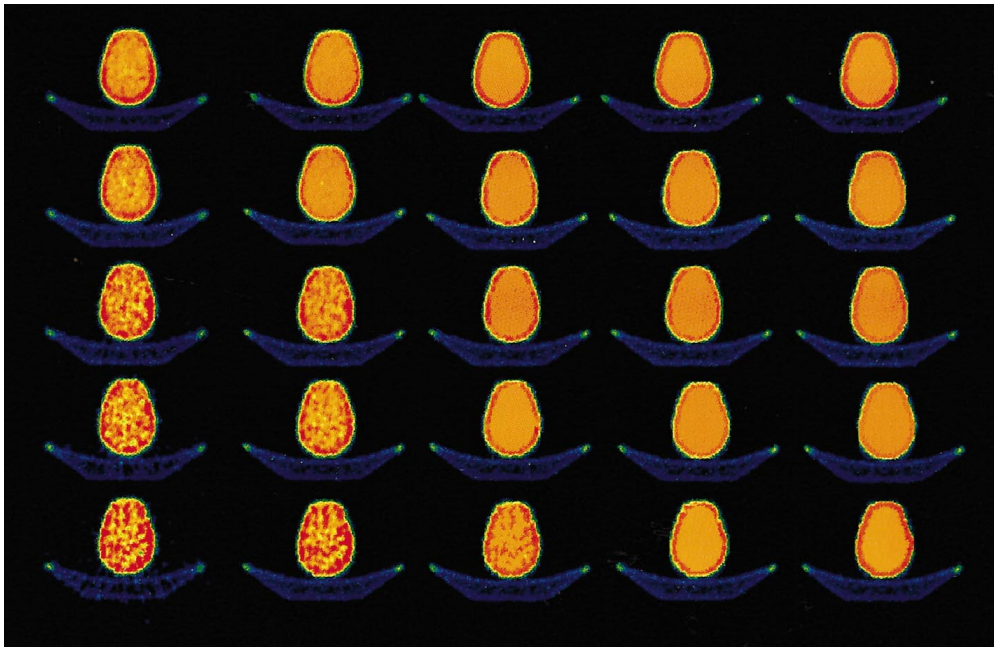

Fig. 5. Rando phantom (head region). Unprocessed (first column) and classified TR images as a function of the acquisition time (60, 30, 15, 5, 3 min – *from top to bottom*) and β values used for the classification (β = 2.0, 1.0, 0.8, 0.4 from the second column, *left to right*). Classification was performed using the two-step procedure

values found with the non-adaptive procedure and noise (SD) is less than or comparable to noise in the reference (60 min) unprocessed TR images.

Human studies

Data acquisition

In order to assess the efficacy of the clustering technique in clinical applications, two brain, two heart and two whole-body fluorine-18 fluorodeoxyglucose ([^{18}F]FDG PET studies were considered.

For the brain studies, the acquisition protocol was as follows:
– Two subsequent TR scans (12 min and 3 min) were recorded. Summed together they produce a 15 min TR scan as in the standard clinical protocol.
– 10-min EM scan, acquired 45 min after the tracer injection (100 μCi/kg body weight).

For the heart studies, the acquisition protocol was as in the brain studies but two TR scans, 17 min and 3 min long, were recorded (summed to produce a 20-min scan as in clinical protocols).

The two whole-body studies consisted of five and seven adjacent EM scans respectively (5 min/bed position, from the head to the feet) performed 1 h after tracer administration. After the EM scans, a 3-min post-injection TR scan (PJ-TR) was performed for each of the five and seven bed positions.

Data analysis

Brain and heart studies were corrected for attenuation using:
a) Summed unclassified TR data (reference data)
b) "Short" (3-min) TR data classified according to the optimised procedure described in the section "Adaptive behaviour of the clustering technique".

Whole-body studies were reconstructed without AC and with AC using the classified PJ-TR data. EM data were reconstructed using an EM-ML algorithm (20 iterations) [25].

Circular ROIs (two pixels in diameter) were drawn on the reconstructed EM images in areas of clinical relevance (cortical and subcortical regions for brain, myocardial wall for heart) over several image planes and average counts/pixel were calculated for each ROI. %Mean difference (signed, $\%MD_S$ and absolute, $\%MD_A$) between ROI values obtained in the EM images corrected for attenuation using the unclassified reference (UR) and classified 3-min (CL) TR data were calculated as:

$$\%MD_s = \sum_{i=1}^{N_{ROIs}} \frac{(UR_i - CL_i)}{UR_i} 100, \quad (9)$$

$$\%MD_A = \sum_{i=1}^{N_{ROIs}} \frac{|UR_i - CL_i|}{UR_i} 100. \quad (10)$$

Profiles through the TR images were drawn to compare edges in the unprocessed and classified TR images and to evaluate the effect of clustering on preserving the edges.

Corrected and uncorrected whole-body studies were qualitatively evaluated by visual inspection by an expert physician.

Results

Brain studies. Four representative TR and EM images of a brain PET study are shown in Fig. 6a and b. $\%MD_S$

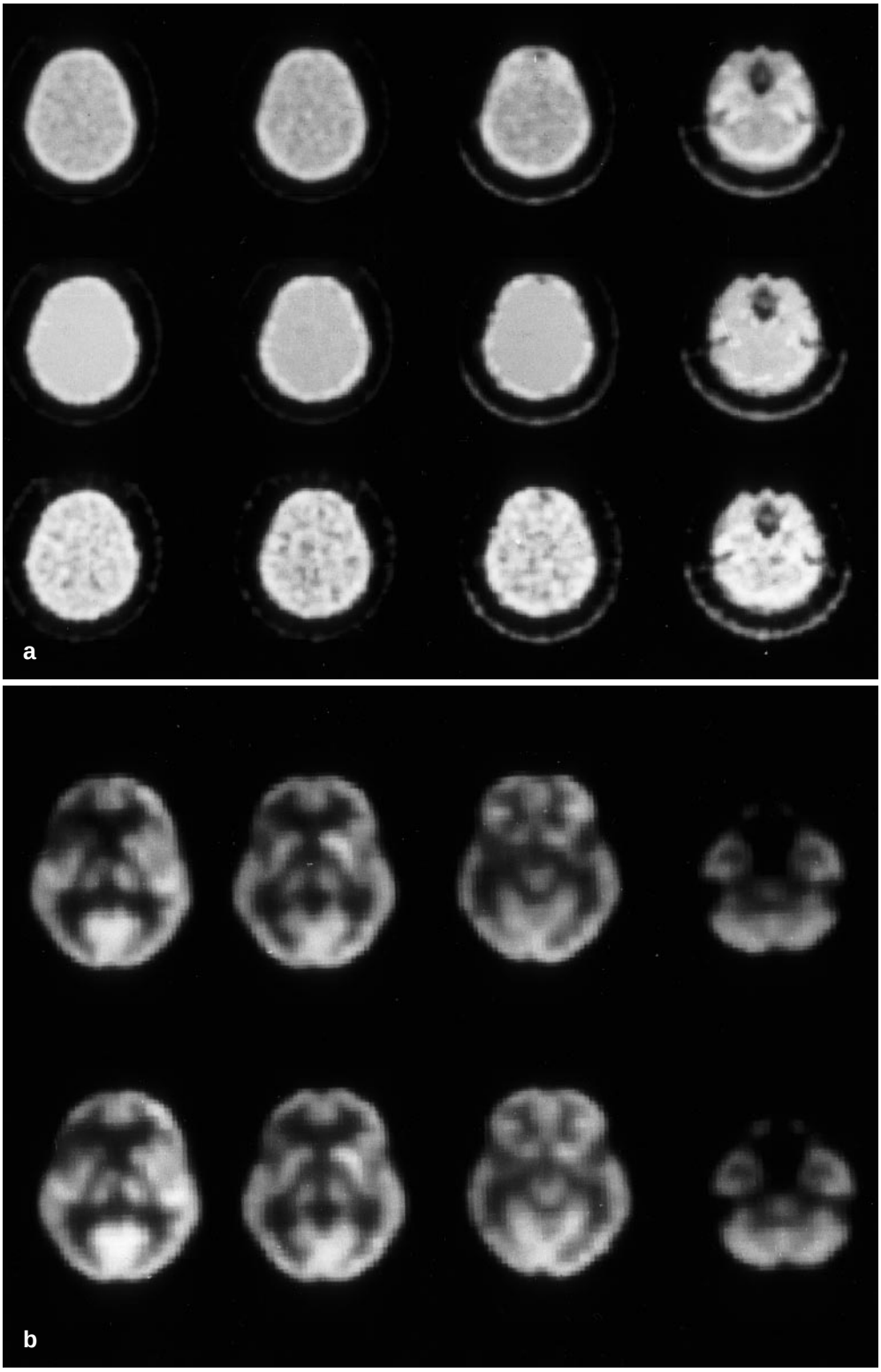

Fig. 6. a Four representative unprocessed (15 min, *top row*, 3 min, *bottom row*) and classified (3 min, *central row*) TR images of a brain PET study. **b** Four representative EM images of a PET brain study. The EM images were reconstructed using for AC the unprocessed (15 min, *top row*) and the classified (3 min, *bottom row*) TR data

and $\%MD_A$ were –1.2% and 2.5% for the first brain study, and 3.1% and 3.5% for the second.

Heart studies. Four representative TR and EM images of two heart PET studies are shown in Fig. 7a and b. $\%MD_S$ and $\%MD_A$ were –4.6 and 5.8% for the first heart study, and –4.5% and 6.0% for the second. The profiles drawn through an unprocessed and a classified TR images are shown in Fig. 7c. As can be seen, the metric and the edges of the original data are well preserved in the classified TR image.

Whole-body studies. In Fig. 8 transaxial, coronal and sagittal images of a whole-body study reconstructed

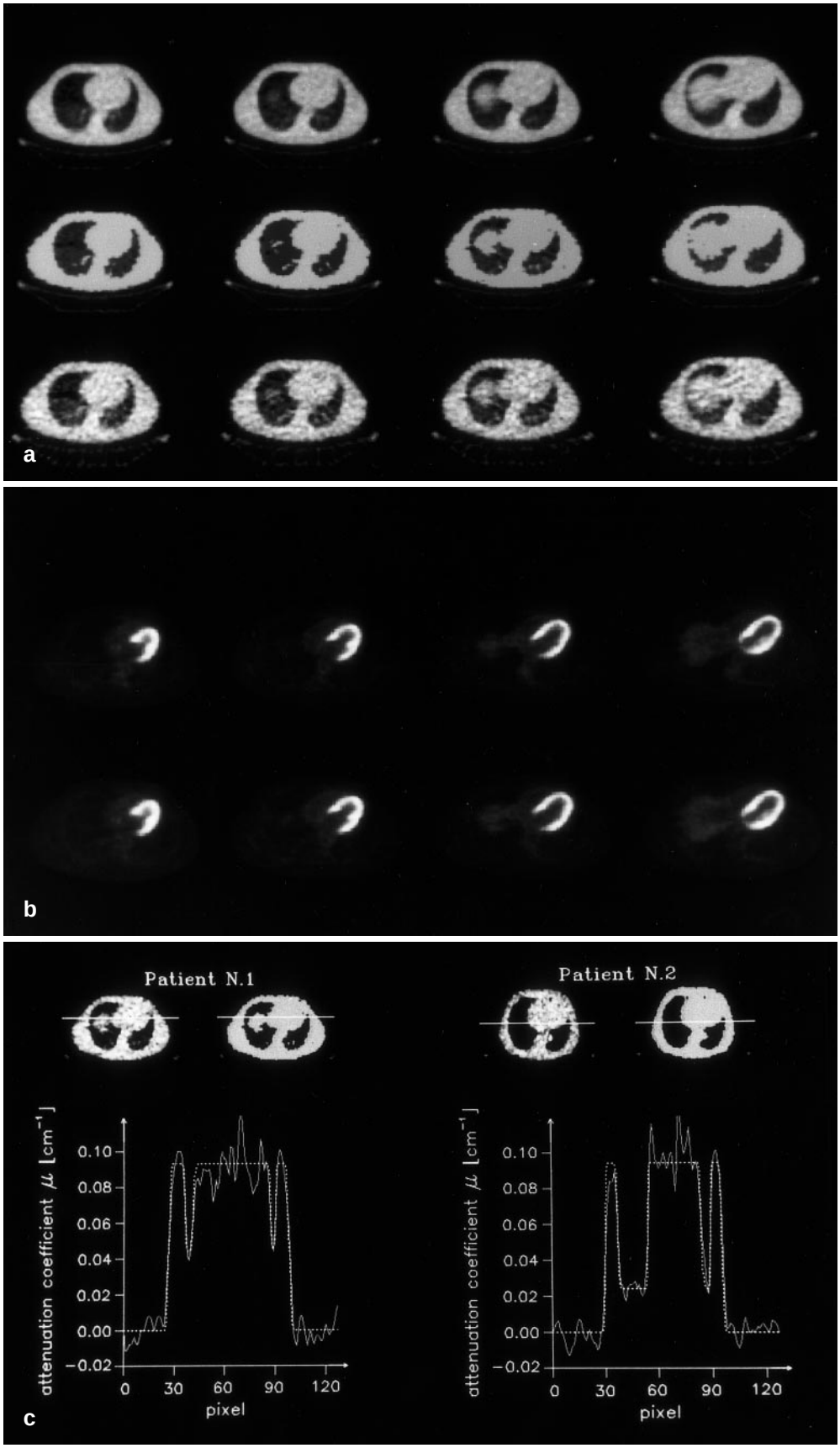

Fig. 7. a Four representative unprocessed (20 min, *top row*, 3 min, *bottom row*) and classified (3 min, *central row*) TR images of a heart PET study. **b** Four representative EM images of a PET heart study. The EM images were reconstructed using for AC the unprocessed (20 min, *top row*) and the classified (3 min, *bottom row*) TR data. **c** Profiles drawn through a representative TR image (unprocessed, *left*; classified, *right*) of two heart studies

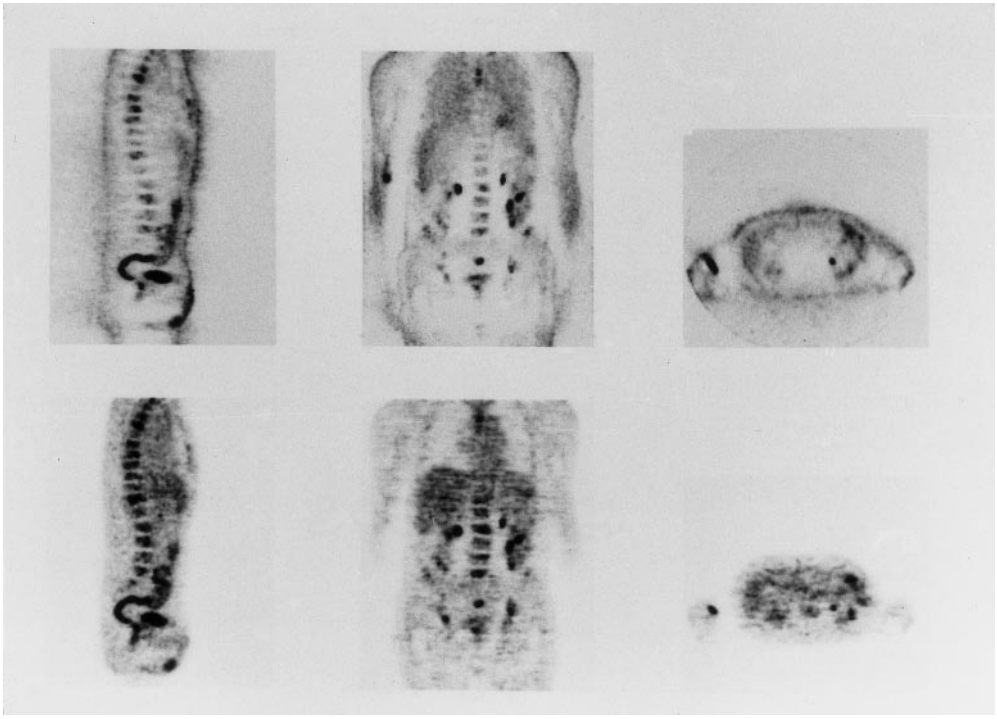

Fig. 8. Sagittal, coronal and transverse EM images of a whole-body study reconstructed without AC (*top*) and with AC (*bottom*) using the classified PJ-TR data

without and with AC are shown. Uncorrected images show an apparent reduction of the tracer uptake in the deep part of the body due to photon attenuation. AC images show a better definition of the body anatomy (lungs, mediastinum, liver, kidney), allowing easier location of high metabolic activity. Metastatic lesions in the spine are more clearly identified in the AC images. Distortions of the image in regions of particularly high uptake are compensated by AC.

Discussion

In this paper a clustering technique for attenuation correction in PET is proposed. The method allows the classification of TR images into the main anatomical regions of the body in terms of corresponding μ values.

A distinguishing feature of the method with respect to other classification techniques proposed in the literature is that the number of classes and their centroids are automatically determined with no *a priori* assumption. The method accounts for the count statistics in TR images by automatically setting a scale parameter β. Furthermore the method is adaptive with respect to the body regions under classification (head, body).

In order to make the method fully automatic, two parameters were empirically determined and fixed: the threshold for background removal and the maximum linear distance, MLD.

– A threshold value of 0.035 cm^{-1} was fixed for a general use of the technique: (a) to be conservative with respect to background level in different noise conditions, and (b) to be low with respect to attenuation coefficients in the body (0.095 cm^{-1} in soft tissue and ≈0.125 cm^{-1} in the skull), thus not affecting recognition of body edges. In the case of a specific acquisition protocol, fine tuning of the threshold parameter can be done and the new value easily implemented.

– The MLD parameter was fixed considering the application of the classification technique to adult subjects. It can be easily changed in the case of paediatric studies.

The method has been implemented in an efficient way (graphical method and histogram approach) to speed up the research of the cluster centres and the data association, which represent the computational core of the classification technique. The program was written in C and runs on a SUN Sparc station 20. Computational time for the classification technique is ≈1 min for 35 TR images.

The classification technique was validated:

a) On TR data of an anthropomorphic phantom in terms of attenuation coefficient and noise level. The method proved to be accurate within 5% in classifying tissue components in both the head and the thorax. In this study, the accuracy of the technique was not assessed in terms of absolute radioactivity concentration, to avoid potential bias due to other physical effects (e.g. randoms, scatter, partial volume effect).

b) On [^{18}F]FDG clinical studies, by comparing EM images corrected for attenuation by classified and unprocessed reference TR data. Differences were within 6%.

Limitations of the classification method were found for very low β values, usually determined when the count statistics of TR data is very poor. Few classes are then recognised by the algorithm and “small” details and smooth transitions between regions with different atten-

uation coefficients can be lost. In particular, this situation can occur at the end regions of the interfaces between liver and lungs. A comparison of the classified with the original TR images can be useful to recognise these local classification errors, which might produce spatially correspondent errors in the reconstructed EM images.

In conclusion, this work indicates that short TR scans (down to 3 min for normal activity in the TR pin sources) can be accurately classified and used for improving measured AC in PET. The method proposed is fast and unsupervised, and is thus particularly feasible for applications in a PET clinical environment.

References

1. Huang SC, Hoffman EJ, Phelps ME, Kuhl DE. Quantitation in positron emission computed tomography. 2. Effects of inaccurate attenuation correction. *J Comput Assist Tomogr* 1979; 3: 804–814.
2. Dahlbom M, Hoffman EJ. Problems in signal-to-noise ratio for attenuation correction in high resolution PET. *IEEE Trans Nucl Sci* 1987; 34: 288–292.
3. Ostertag H, Kubler WK, Doll J, Lorenz WJ. Measured attenuation correction methods. *Eur J Nucl Med* 1989; 15: 722–726.
4. Thompson CJ, Ranger NT, Evans AC. Simultaneous transmission and emission scan in positron emission tomography. *IEEE Trans Nucl Sci* 1989; 36: 1011–1016.
5. Thompson CJ, Ranger NT, Evans AC, Gjedde A. Validation of simultaneous PET emission and transmission scans. *J Nucl Med* 1990; 32: 154–160.
6. Meikle SR, Bailey DL, Hooper PK, Eberl S, Hutton BF, Jones WF, Fulton RR, Fulham MF. Simultaneous emission and transmission measurements for attenuation correction in whole-body PET. *J Nucl Med* 1995; 36: 1680–1688.
7. Meikle SR, Eberl S, Hopper PK, Fulham MJ. Simultaneous emission and transmission scanning in PET oncology: the effect on parameter estimation. *IEEE Trans Nucl Sci* 1997; 44: 67–73.
8. Thompson CJ, Dagher A, Lunney DN, Strother SC, Evans AC. A technique to reject scattered radiation in PET transmission scans. In: Nalcioglu O, Cho ZH, Budinger TF, eds. International workshop on physics and engineering of computerized multidimensional imaging and processing. *Proc SPIE* 1986; 671: 244–253.
9. Huesman RH, Derenzo SE, Cahoon JL, Geyer AB, Moses WW, Uber DC, Vuletich T, Budinger TF. Orbiting transmission source for positron tomography. *IEEE Trans Nucl Sci* 1988; 35: 735–739.
10. Kubler WK, Ostertag H, Hoverath H, Doll J, Ziegler S, Lorenz W. Scatter suppression by using a rotating pin source in PET transmission measurements. *IEEE Trans Nucl Sci* 1988; 35: 749–756.
11. Daube-Witherspoon ME, Carson RE, Green MV. Post-injection transmission attenuation measurements for PET. *IEEE Trans Nucl Sci* 1988; 35: 757–761.
12. Carson RE, Daube-Witherspoon ME, Green MV. A method for post-injection PET transmission measurements with a rotating source. *J Nucl Med* 1988; 29: 1558–1567.
13. Ranger NT, Thompson CJ, Evans AC. The application of a masked orbiting transmission source for attenuation correction in PET. *J Nucl Med* 1989; 30: 1056–1068.
14. Luk WK, Digby WD, Jones WF, Casey ME. An analysis of correction methods due emission contamination in PET post-injection transmission measurement. *IEEE Trans Nucl Sci* 1995; 42: 2303–2308.
15. Karp JS, Muehllehner G, He Qu, Yan X-H. Singles transmission in volume-imaging PET with a ^{137}Cs source. *Phy Med Biol* 1995; 40: 929–944.
16. Huang SC, Carson RE, Phelps ME, Hoffman EJ, Schelbert HR, Kuhl DE. A boundary method for attenuation correction in positron computed tomography. *J Nucl Med* 1981; 22: 627–637.
17. Xu EZ, Mullani NA, Gould LK, Anderson WL. A segmented attenuation correction for PET. *J Nucl Med* 1991; 32: 161–165.
18. Ollinger JM. Reconstruction-reprojection processing of transmission scans and the variance of PET images. *IEEE Trans Nucl Sci* 1992; 39: 1122–1125.
19. Stearns CW, Wack DC. A noise equivalent counts approach to transmission imaging and source design. *IEEE Trans Nucl Sci* 1993; 12: 287–292.
20. Meikle SR, Dahlbom M, Cherry SR. Attenuation correction using count-limited transmission data in positron emission tomography. *J Nucl Med* 1993; 34: 143–150.
21. Tai YC, Lin KP, Dahlbom M, Hoffman EJ. A hybrid attenuation correction technique to compensate for lung density in 3-D total body PET. *IEEE Trans Nucl Sci* 1996; 43: 323–330.
22. Xu M, Cutler PD, Luk WK. Adaptive, segmented attenuation correction for whole-body PET imaging. *IEEE Trans Nucl Sci* 1996; 43: 331–336.
23. Beni G, Liu X. A least biased fuzzy clustering method. *IEEE Trans Pattern Anal Machine Intell* 1994; 16: 954–960.
24. Khan FM. The physics of the radiation therapy. Baltimore: Williams & Wilkins; 1994; 177–178.
25. Lange K, Carson R. EM reconstruction algorithms for emission and transmission tomography. *J Comput Assist Tomogr* 1984; 8: 306–316.